Thallium-201/Technetium-99m-Phytate (Colloid) Subtraction Imaging of Hepatocellular Carcinoma

Teruhito Mochizuki, Tomoko Takechi, Kenya Murase, W. Newlon Tauxe, Harold A. Bradfield, Shuji Tanada and Ken Hamamoto

Departments of Radiology Imabari Ehime Hospital, Ehime University School of Medicine, Ehime, Japan and University of Pittsburgh School of Medicine, Pittsburgh, Pennsylvania

This paper evaluates the clinical usefulness of ^{201}Tl to image hepatocellular carcinoma (HCC), using ^{201}Tl, ^{99m}Tc-phytate (colloid) and a three-headed SPECT camera. **Methods:** The tumor-to-nontumor ratios (T/N) of ^{201}Tl for different categories of HCC were generated. Tumors were emphasized by image subtraction (^{201}Tl-^{99m}Tc-colloid). Thirty-three lesions in 16 patients (18 studies) with HCC were evaluated. There were 19 untreated nodular, five untreated diffuse, five local recurrent and four necrotic lesions after interventional therapy. **Results:** The mean T/N were as follows: untreated nodular 1.54 ± 0.31 (mean ± s.d.), untreated diffuse 1.28 ± 0.26, local recurrence 1.50 ± 0.29 and necrosis 0.22 ± 0.06. All the tumors (except necrotic areas) were enhanced by the image subtraction. **Conclusion:** Thallium-201 is useful for liver tumor imaging but ^{99m}Tc-phytate (colloid) is essential to discriminate ^{201}Tl tumor uptake from normal liver accumulation. Image subtraction (^{201}Tl/^{99m}Tc-colloid) is helpful in detecting HCC.

Key Words: thallium-201; technetium-99m-phytate; SPECT; subtraction images; hepatocellular carcinoma

J Nucl Med 1994; 35:1134–1137

Several diagnostic modalities to image hepatocellular carcinoma (HCC) are currently available. Ultrasound (US) and CT are the most popular noninvasive imaging modalities for screening of HCC, and MRI is playing a complementary role in diagnosing HCC. US and CT usually depict HCC well, however, they may depict questionable lesions as well. Nuclear medicine has been providing a complementary role to evaluate these questionable lesions with high tumor-to-nontumor contrast imaging techniques such as ^{67}Ga for positive agents and colloid liver scans for negative agents in terms of metabolism and function. Thallium-201 has recently been powerfully investigated as a possible imaging agent and proved to be useful for many kinds of tumors (*1–11*) and may be useful for imaging HCC as well. Therefore, we hypothesized that ^{201}Tl can substitute for ^{67}Ga as a positive agent in imaging HCC with higher resolution and ^{99m}Tc-colloid liver SPECT assists in detecting lesions as a negative agent. A combination of dual-energy acquisition and high-resolution three-headed SPECT is probably the best tool for evaluating these hypotheses generally available today. The authors tried to emphasize the liver tumors by eliminating the surrounding liver accumulation with an image subtraction technique (^{201}Tl/^{99m}Tc-phytate colloid).

Received Jan. 14, 1994; accepted Mar. 23, 1994.

For correspondences and reprints contact: Teruhito Mochizuki, MD, Radiology, Ehime Imabari Hospital, 4-5-5 Ishii-cho, Imabari-city, Ehime 794, Japan.

MATERIALS AND METHODS

Thirty-three lesions in 16 patients (18 studies) were evaluated in Table 1. Lesions were classified into four categories: (1) untreated nodular lesions, including daughter lesions; (2) untreated diffuse lesions; (3) local recurrences; and (4) necroses after interventional therapy. The lesions were depicted by plain and/or contrast-enhanced CT. All except necroses were diagnosed by angiography, including lipiodol CT (CT after transarterial lipiodol injection) and/or CT-AP (trans-superior-mesenteric-arterial portography CT). The lesions were clinically confirmed by more than 6-mo follow-up. In the necrosis group, there were no local recurrences for at least 6 mo. Most of the tests were performed complementarily to evaluate the questionable lesions depicted by CT or to increase the confidence level of the CT diagnosis before angiography and/or interventional therapy in the clinical setting. Ages ranged from 45 to 76 yr with a mean of 61 yr. There were 15 males (16 studies) and one female (two studies).

The SPECT system used was a Toshiba GCA-9300A (Toshiba, Japan), having three detectors equipped with low-energy, high-resolution, parallel-hole collimators and a Toshiba GMS-550U processor. Matrix size was 128 × 128 and the slice thickness was 3.2 mm. The two-dimensional filter was a 15 × 15 Butterworth (order = 8, 0.15 cycles/pixel) and the ECT filter was a Shepp and Logan. The mean radius of rotation was 210 mm.

Patients were injected intravenously with 111 MBq of ^{201}Tl and were placed on the imaging table 30 min later. The first set of data was acquired using only a single energy peak of the ^{201}Tl (71 keV ± 10%). The detector system rotated over 120° in twenty 30-sec steps, for 12 min. Soon after the first acquisition, 185 MBq of ^{99m}Tc-phytate was injected and 10 min later the second set of data was acquired using dual-energy mode, one for each nuclide (^{201}Tl 71 keV ± 10%; ^{99m}Tc 140 keV ± 10%). Patients were instructed not to move during and between the single-mode and dual-mode

TABLE 1
Patient Data

Patient	Age	Sex	No. of lesions: Untreated nodular	Untreated diffuse	Recurrence	Necrosis
1	62	M			1	1
2	72	M	7			
3	61	M	1			
4	62	M	1	2		1
5-1	70	M	1			
5-2	70	M				1*
6	56	M			1	
7	65	M	1			
8	61	M			2	1
9	76	M	2			
10	63	M	1	1		
11	47	M	1	1		
12	62	M			1	
13	64	M	1			
14	51	M	1			
15	45	M		1		
16-1	59	F	1			
16-2	60	F	1†			

*The second study was performed 3-wk after transcatheter arterial embolization, i.e., 1 mo after the first study (5-1).

†The follow-up study was performed 1 yr after the first study (16-1) and operation.

scans to minimize artifacts. Acquisition conditions were the same for both modes. Three sets of projection data, i.e., single-mode ^{201}Tl, dual-mode ^{201}Tl and ^{99m}Tc-phytate, were reconstructed to transaxial images using the backprojection method. Coronal images were also generated from the transaxial images. There was no correction for attenuation.

Technetium-99m-phytate and two sets of ^{201}Tl images were compared slice-by-slice on the screen and films. Regions of interest (ROIs) were drawn around the photopenic areas (3 × 3 pixel size) seen on the ^{99m}Tc-phytate images and on nontumor control areas (5 × 5 pixel size) as well, avoiding areas of large vessels. These ROIs were superimposed in registry onto the corresponding ^{201}Tl images. The nontumor control area ROIs were used to calculate ratios. Then tumor and nontumor ratios (T/N) in each category were generated, using single-mode ^{201}Tl images (T/N = mean pixel counts of the tumor-to-mean pixel counts of the nontumor). The relationship between the T/N and the tumor size was also investigated. After confirmation that there was no patient movement between the first and the second sets of ^{201}Tl images, by comparing the two sets of ^{201}Tl images on the film, the phytate images were subtracted from single-mode ^{201}Tl images (^{201}Tl/^{99m}Tc) in all slices. The constant for subtraction which is multiplied to colloid images was decided after three to five experimental subtractions at the center of the tumor.

Statistical significance of differences among the categorical T/N was analyzed by ANOVA using 95% as a criterion for significance.

RESULTS

T/N ratios by diagnostic category are summarized in Figure 1. In untreated nodular lesions, the T/N ratio was 1.54 ± 0.31 (mean ± s.d.); in untreated diffuse lesions, the T/N ratio was 1.28 ± 0.26; in local recurrences, the T/N ratio was 1.50 ± 0.29; and in necrotic areas, the T/N ratio was 0.22 ± 0.06. The T/N ratio of those areas was significantly lower than those of others. The T/N ratios of untreated nodular lesions, untreated diffuse lesions and local recurrence were not significantly different from each other. All the tumors, except necrotic areas, were highlighted by the image subtraction. T/N ratio versus tumor size is plotted in Figure 2. In general, poor correlation between the T/N ratio and the tumor size was observed. Representative cases are shown in Figures 3–8. An untreated small (2 cm in diameter) nodular HCC is shown in Figures 3 and 4. Pre- and post-transarterial embolization therapy (TAE) of an untreated nodular HCC is shown in Figures 5 and 6. An untreated diffuse HCC is shown in Figures 7 and 8.

DISCUSSION

Liver tumors have usually been screened and detected well by US and CT. However, small or diffuse HCC is sometimes difficult to detect in the cirrhotic liver by either US or CT. US may miss a tumor at the marginal area near

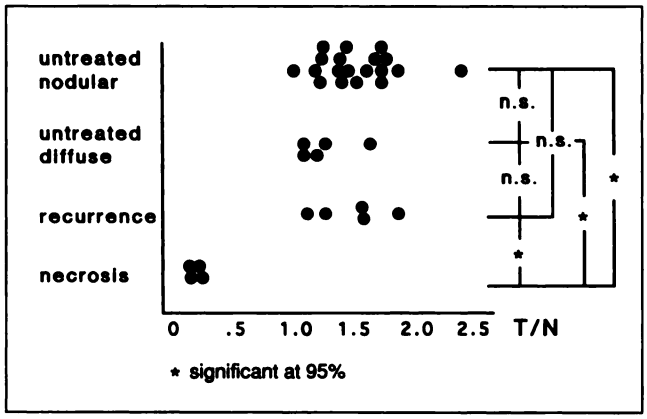

FIGURE 1. Graph of T/N ratios by category in HCC. The T/N of the necrotic lesions was significantly lower than non-necrotic HCC.

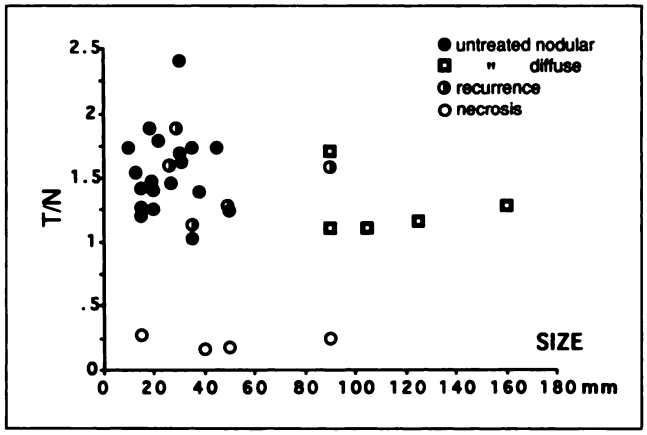

FIGURE 2. Graph of T/N ratios versus tumor size. The T/N does not correlate well with the tumor size.

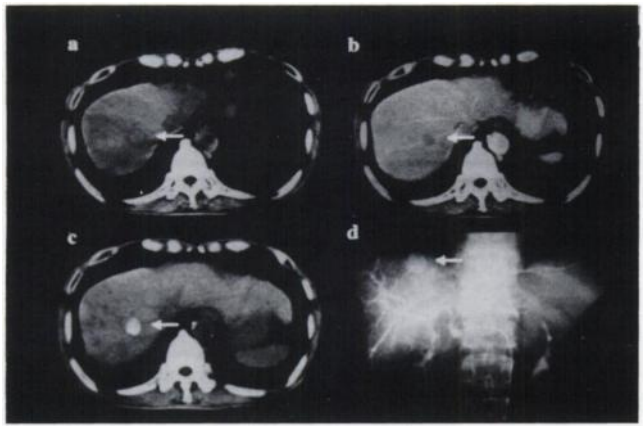

FIGURE 3. Data from a 65-yr-old male patient (Patient 7) with nodular hepatocellular carcinoma (HCC). Plain (a) and contrast enhancement (b) CT depict a small tumor (←, 2 cm in diameter) near the dome of the liver. (c) A small amount of lipiodol was injected through a transarterial catheter for diagnostic purposes and was accumulated in the HCC by CT (←). (d) Angiogram of the late arterial phase demonstrates a stain of the tumor (←).

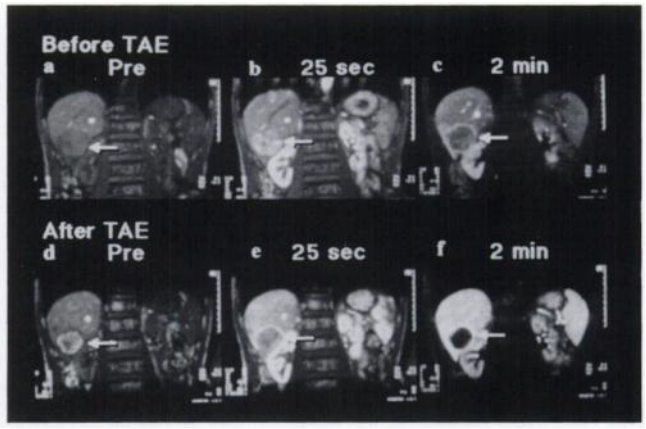

FIGURE 5. Data from a 70-yr-old male patient (Patient 5) pre- and post-transarterial embolization (TAE) of nodular hepatocellular carcinoma (HCC). Pre-TAE dynamic MRI (FL2D TR/TE/FA, 74/6/80) depicts the HCC as an area of increased arterial blood supply: (a) predynamic, (b) 25 sec and (c) 2 min. Post-TAE dynamic MRI (FL2D TR/TE/FA, 90/6/80) demonstrates no perfusion to the treated HCC: (d) predynamic, (b) 25 sec and (c) 2 min.

the dome and CT is likely to miss an isodensity tumor or may not obtain a consecutive image due to erratic breath holding.

Because of its high attenuation on CT, and the high accumulation throughout the normal liver, it is difficult to assess HCC viability (i.e., size) or perfusion soon after the injection of the frequently used embolic agent lipiodol. Moreover, the characterization of the tumor by CT (or US) is nonspecific. Therefore it is useful to develop a different strategy in detecting liver tumors and in evaluating tumor viability after intervention therapy.

Thallium-201 was reported as a possible agent for tumor imaging (*1–3*) and its clinical usefulness for many kinds of tumors has been recently investigated (*4–11*). HCC was reported to accumulate ^{201}Tl with planar images (*12,13*). However, normal physiological accumulation of the ^{201}Tl to the liver is an annoying problem to evaluate the smaller HCC in planar images. Thereafter, no further investigation was reported. The recently introduced three-headed high-resolution SPECT camera has emphasized the benefit of nuclear medicine imaging in evaluating smaller lesions which may not be detected with planar images. However, the uptake of HCC is often as intense as the surrounding liver accumulation, even though the tumor uptake may be slightly higher, it may not be possible to detect a lesion with assurance. Therefore, the assistance of ^{99m}Tc-phytate (colloid) was quite helpful in detecting the tumor as a decreased intensity area and to identify the ^{201}Tl tumor uptake, especially in small or diffuse HCC.

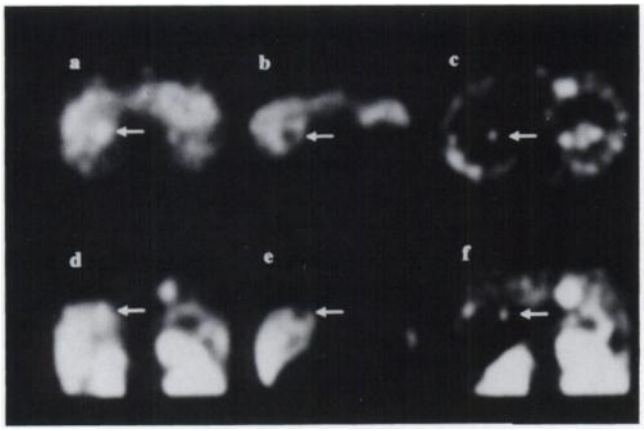

FIGURE 4. Data from the same patient as Figure 3. (a) Transaxial ^{201}Tl image shows an area of high intensity (←). (b) On the other hand, the ^{99m}Tc-phytate (colloid) image demonstrates an area of decreased intensity (←). (c) The subtraction image shows a small hepatocellular carcinoma (←). (d) Coronal images of ^{201}Tl, (e) ^{99m}Tc-phytate, and (f) a subtraction.

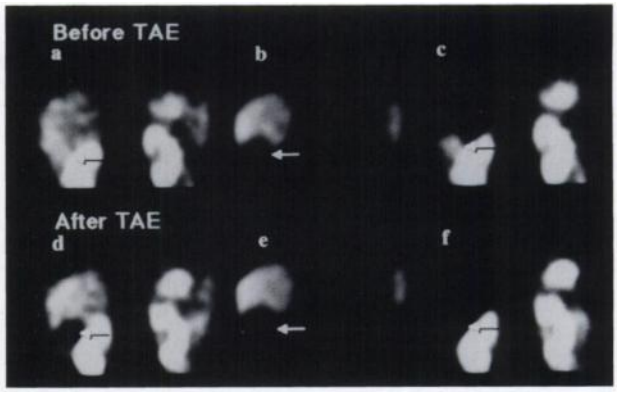

FIGURE 6. Data from the same patient as Figure 5. (a) Pre-transarterial embolization (TAE) ^{201}Tl image shows an area of slightly increased intensity (←) where (b) ^{99m}Tc-phytate image shows an area of decreased intensity (←). (c) After subtraction, the hepatocellular carcinoma (HCC) was clearly visible (←). (d) Post-TAE ^{201}Tl image shows an area of decreased intensity (←) where (e) the ^{99m}Tc-phytate image also showed an area of decreased intensity (←). (f) After subtraction, no HCC was visible (←).

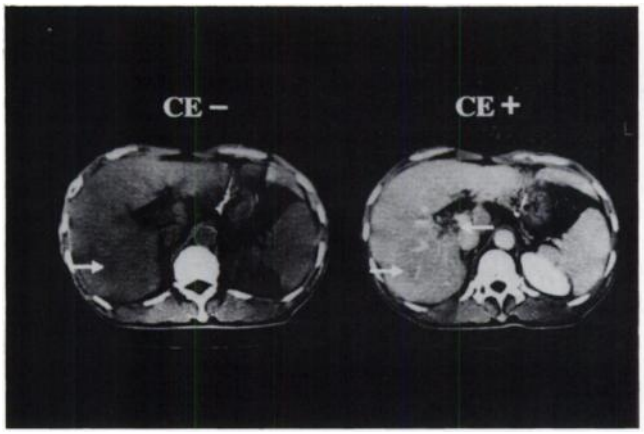

FIGURE 7. Data from a 63-yr-old male patient (Patient 10) with diffuse HCC. The diffuse HCC lesion remains poorly differentiated on either plain (CE –) or contrast enhancement (CE +) CT (←). A small defect of the tumor thrombus in the portal vein is evident on contrast enhancement CT (←).

As shown in the representative cases in Figures 3–8, image subtraction (^{201}Tl-^{99m}Tc-phytate colloid) highlighted the liver tumor by eliminating the surrounding liver accumulation. Since ^{99m}Tc-phytate is commercially available and easy to handle in Japan, it was used for liver colloid scans in this series, however, ^{99m}Tc-sulfur colloid can be used as well.

The idea of image subtraction for depicting tumors could be applied to other kinds of tumors using various kinds of radionuclides (*14*). Image fusion (*15*) (^{201}Tl or ^{99m}Tc images to CT) was also quite helpful in confirming that the lesion of increased ^{201}Tl uptake or decreased ^{99m}Tc uptake matches the lesion in CT. Adjusting the image size of ^{201}Tl and ^{99m}Tc to CT, we superimposed ^{201}Tl and ^{99m}Tc images on the screen. Since there are many markers for slice identification such as the heart, liver, spleen, stomach and kidneys with ^{201}Tl images, and liver and spleen with ^{99m}Tc-colloid images, it was not difficult to fuse the different kinds of images, once the size was properly adjusted. We speculate that the same idea may be applied to the renal tumor imaging using ^{201}Tl as a positive agent and ^{99m}Tc-dimercaptosuccinic acid (DMSA) as a negative agent in discriminating renal tumors such as renal cell carcinoma from benign lesions such as column of Bertin, lobulation or a high-density cyst on CT, among others.

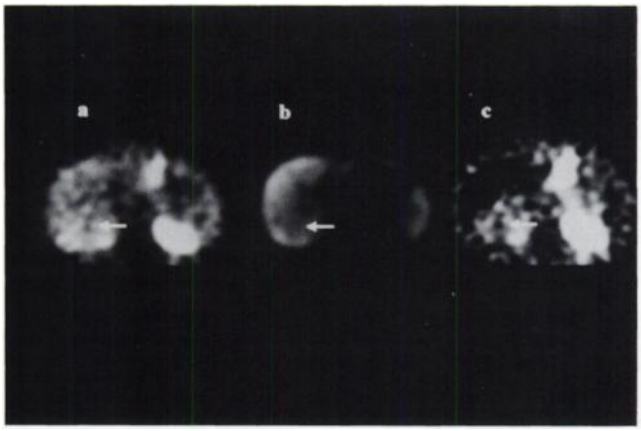

FIGURE 8. Data from the same patient as in Figure 7. (a) Thallium-201 image shows an area of increased intensity (←) where (b) the ^{99m}Tc-phytate image showed an area of decreased intensity (←). (c) After subtraction, diffuse HCC was clearly emphasized (←).

The T/N ratio of the necrotic group after interventional therapy was significantly lower than the others, which is helpful in evaluating the effectiveness of the interventional therapy and in depicting the local recurrence. There was not a strong relationship between tumor size and the T/N ratio in untreated HCC. This may suggest that the activity or grade of malignancy of the tumor may not depend on size. Unfortunately, it is often difficult to obtain tissue from HCC patients in the clinical setting; thus we only obtained tissue from three patients in this study. Histological correlation with the T/N ratio or relationship between the growing speed (doubling time) and the T/N ratio therefore remains to be studied in a long-range study in the future.

ACKNOWLEDGMENT

This work was presented in part at the 39th Annual Meeting of the Society of Nuclear Medicine in Los Angeles, CA, 1992 and at the 40th Annual Meeting of the Society of Nuclear Medicine in Toronto, Canada, 1993.

REFERENCES

1. Salvatore M, Carratu L, Porta E. Thallium-201 as a positive predictor for lung neoplasm: preliminary experience. *Radiology* 1976;121:487–488.
2. Cox PH, Belfer AJ, Van der Pompe WB. Thallium-201 chloride uptake in tumors, a possible complication in heart scintigraphy. *Br J Radiol* 1976;49: 767–768.
3. Tonami N, Hisada K. Clinical experience of tumor imaging with ^{201}Tl-chloride. *Clin Nucl Med* 1977;2:75–81.
4. Basara BE, Wallner RJ, Hakki AH, Iskandrian AS. Extracardiac accumulation of thallium-201 in pulmonary carcinoma. *Amer J Cardiol* 1984;53: 358–359.
5. Hoeinagel CA, Delprat CC, Marcuse HR, de Vijlder JM. Role of thallium-201 total body scintigraphy in follow-up of thyroid carcinoma. *J Nucl Med* 1986;27:1854–1857.
6. Kaplan WD, Takuborian T, Morris JH, Rumbaugh CL, Connolly BT, Atkins HL. Thallium-201 brain tumor imaging: a comparative study with pathologic correlation. *J Nucl Med* 1987;28:47–52.
7. El-Gazzar AH, Sahweil A, Abdel-Rahim SM, et al. Experience with thallium-201 imaging in head and neck cancer. *Clin Nucl Med* 1988;13:286–289.
8. Oriuchi N, Tamura M, Shibazaki T, et al. Clinical evaluation of thallium-201 SPECT in supratentorial gliomas: relationship to histologic grade, prognosis and proliferative activities. *J Nucl Med* 1993;34:2085–2089.
9. Tonami N, Hisada K. Thallium-201 in the evaluation of gliomas. *J Nucl Med* 1993;34:2089–2090.
10. Jinnouchi S, Hoshi H, Ohnishi T, et al. Thallium-201 SPECT for predicting histological types of meningiomas. *J Nucl Med* 1993;34:2091–2094.
11. Lee VW, Sax EJ, McAneny DB, et al. A complementary role for thallium-201 scintigraphy with mammography in the diagnosis of breast cancer. *J Nucl Med* 1993;34:2095–2100.
12. Hisada K, Tonami N, Miyamae T, et al. Clinical evaluation of tumor imaging with thallium-chloride. *Radiology* 1978;129:497–500.
13. Tonami N, Nakajima K, Hisada K, et al. Thallium-201 per-rectal scintigraphy in primary hepatocellular carcinoma. *J Nucl Med* 1985;6:327–339.
14. Bradfirld HA, Tauxe WN, Levine G, Kirkwood JM, Klein H, Mochizuki T. Indium-111-labeled monoclonal antibody versus gallium-67-citrate and technetium-99m-sulfur colloid subtraction in a case of malignant melanoma. *Clin Nucl Med* 1994: in press.
15. Wahl RL, Quint LE, Cieslak RD, Aisen AM, Koeppe RA, Meyer CR. "Anatometabolic" tumor imaging: fusion of FDG PET with CT or MRI to localize foci of increased activity. *J Nucl Med* 1993;34:1190–1197.